Journal of Colloid and Interface Science 545 (2019) 54–62

Contents lists available at ScienceDirect

Journal of Colloid and Interface Science

journal homepage: www.elsevier.com/locate/jcis

Editor's Choice

Sub-1 nm PtSn ultrathin sheet as an extraordinary electrocatalyst for methanol and ethanol oxidation reactions

Jee-Yee Chen [a,1], Suh-Ciuan Lim [a,1], Chun-Hong Kuo [b], Hsing-Yu Tuan [a,*]

[a] Department of Chemical Engineering, National Tsing Hua University, Hsinchu 30013, Taiwan
[b] Institute of Chemistry, Academia Sinica, Taipei 11529, Taiwan

GRAPHICAL ABSTRACT

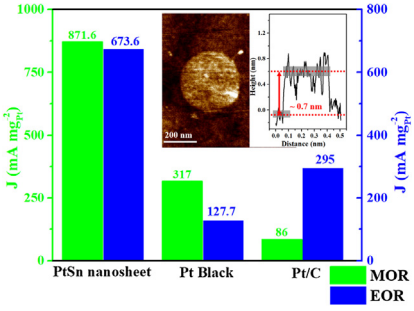

ARTICLE INFO

Article history:
Received 11 January 2019
Revised 24 February 2019
Accepted 25 February 2019
Available online 5 March 2019

Keywords:
Sub-1 nm PtSn nanosheets
Solution colloidal method
Electrooxidation catalysts
Methanol oxidation reaction
Ethanol oxidation reaction

ABSTRACT

Sub-1 nm PtSn nanosheets of 0.6–0.9 nm in thickness were synthesized via a solution colloidal method and were applied as electrooxidation catalysts for methanol oxidation reaction (MOR) and ethanol oxidation (EOR) in alkaline and acid environments. Owing to the specific structural and compositional characteristics, the as-prepared PtSn nanosheets exhibits superior activity and durability relative to commercial Pt black and Pt/carbon catalysts. PtSn nanosheets not only exhibit an outstanding mass activity in MOR (871.6 mA mg Pt^{-1}), which is 2.3 times (371 mA mg Pt^{-1}) and 10.1 times (86.1 mA mg Pt^{-1}) higher than that of commercial Pt/carbon and Pt black respectively, but also display an mass activity in EOR (673.6 mA mg Pt^{-1}) with 5.3 times higher commercial Pt black (127.7 mA mg Pt^{-1}) and 2.3 times higher than commercial Pt/C catalyst (295 mA mgPt^{-1}). The reported value is the highest activity in both MOR and EOR examinations compared to the reported PtSn-based electrocatalysts,. The improved performance may be due to the highly-reactive exposed (1 1 1) facet sites resulted from its sub-1 nm 2D sheet like morphology.

1. Introduction

Electrocatalysts play a major role in the development of direct alcohol fuel cells (DAFCs). Platinum (Pt)-based nanocatalysts are the most promising and active electrode in catalysing the electrochemical reactions, due to their high activity and durability [1–6]. However, the high cost and scarcity of Pt, as well as the critical problem of Pt surfaces poisoning upon formation of reaction intermediates, [7,8] thus limits the practical applications of DAFCs (particularly direct ethanol fuel cells, DEFCs) containing Pt/C catalyst. Therefore, to design of Pt-based electrode catalysts with reduced Pt amount, enhanced catalytic activity and stability is highly desirable. For instance, bimetallic Pt-based electrocatalysts such as PtSn, [9–11] CuPt, [12–14] RuPt, [15–20] RhPt, [21–23]

* Corresponding author.
E-mail address: hytuan@che.nthu.edu.tw (H.-Y. Tuan).
[1] These authors contributed equally to this work.

https://doi.org/10.1016/j.jcis.2019.02.082
0021-9797/

PdPt, [24–27] NiPt [28–32] have been employed for promotion of methanol oxidation reaction (MOR) or ethanol oxidation reaction (EOR) and alleviate catalysts poisoning [33–41].

Particularly, PtSn nanostructures have shown greater catalytic activity than the other reported Pt-based nanocatalysts, because Sn can supply surface oxygen-containing species for the oxidative removal of CO-like species strongly adsorbed on adjacent Pt active sites, which is the so-called bi-functional mechanism that alter the electronic structure of Pt atoms in PtSn nanostructures that favour EOR [42–45]. The presence of Sn component favors the C—C bond breaking at low overpotentials, causing the generation of acetaldehyde and acetic acid at high overpotentials, [46] and can further promote the MOR or EOR on Pt in acid media, [45] and enhance electrooxidation on both Pt and Pd in alkaline media [47].

In order to enhance the atom-utilization efficiencies, regulating the structures of Pt-based nanocatalysts with controllable high-energy facets exposure have recently been of particular interest [48–50]. Among them, ultrathin 2D sheet-like structures with single or few atomic layer thickness (<5 nm) poses excellent catalytic activities, due to their relatively high surface energy, high surface to volume ratio and high density of unsaturated atoms [51]. For instance, the electrocatalytic activity of ultrathin Pt nanosheets showed enhanced catalytic performance for ammonia oxidation compared with the flower-like Pt particles and commercial Pt/C catalyst, [52] and ultrathin PtCu alloy nanosheets demonstrated its higher catalytic activity in hydrogen evolution and hydrogenation reactions compare to spherical PtCu nanoparticles and a commercial Pt black catalyst [53].

Herein, we demonstrate the colloid synthesis of PtSn nanosheets with thickness less than 1 nm for the first time. Sub-1 nm ultrathin PtSn nanosheets with thicknesses ranging from approximately 0.6–0.9 nm were prepared by decomposing tin (IV) iodide (SnI4) and platinum (II) iodide (PtI2) precursor in the presence of a mixture of oleylamine (OLA), trioctylphosphine (TOP), oleic acid (OA) and hexamethyldisilazane (HMDS) under argon atmosphere at 320 °C. The prepared PtSn alloy nanosheets can perform MOR and EOR at both acidic and alkaline media. Significantly, owing to their specific structural and compositional characteristics, PtSn nanosheets outperforming both commercial Pt black and Pt/C catalysts for MOR and EOR, showing 10.1 and 2.3 times higher mass activity toward MOR, 5.3 and 2.3 times higher mass activity toward MOR, respectively.

2. Experimental section

2.1. Chemicals

All chemicals are commercially analytical grade reagents. Tin (IV) iodide (SnI_4; 99.99%), platinum (II) iodide (PtI_2; powder), trioctylphosphine (TOP; 90%), oleylamine (OLA; 70%), oleic acid (OA; 90%), 1-Dodecanethiol (DDT, ≥98%), hexamethyldisilazane (HMDS; ≥99%), toluene (99.5%), methanol (99.5%), ethanol (99.99%), platinum black (Pt black; 40–60 m^2/g, 99.95%) was purchased from Sigma-Aldrich corporation, 20 wt% Pt/Carbon was purchased from Fuel Cell store company.

2.2. Synthesis of PtSn nanosheets

PtSn nanosheets were synthesized in a 50 mL three-neck flask connected to the Schlenk line system under an argon atmosphere. Firstly, 46.4 mg of PtI_2, 6 mL of OLA, and 0.5 mL of TOP were loaded into 50 mL three-neck flask with an argon steam purged under the Schlenk line system, and preheated the mixture solution at 130 °C for 30 min with continuing stirring. Next, sonicated the stock solution which contained 60 mg of SnI_4, 10 mL OLA and 0.75 mL OA into a 20 mL sample vial until dissolve completely. After all the preparation, 1 mL of HMDS and the dissolved stock solution were sequentially injected into the three-neck flask and reheated to 130 °C. Then we heated up the reaction to 320 °C by a rate of 2 °C/min. Once the temperature reached 320 °C, the flask was immediately quenched by a cold water batch instantly to room temperature for stopping the reaction. In order to discard by-products and unreacted precursors, the synthesized nanosheets were washed by centrifugation at 8000 rpm for 5 min with approximately 1:2 v/v toluene and ethanol several times.

2.3. Characterization

The morphologies of PtSn nanomaterials were characterized by a scanning electron microscopy (SEM), an energy-dispersive X-ray spectroscopy (EDS), a transmission electron microscopy (TEM) and an X-ray diffraction (XRD). With a HITACHI-S4800 field-emission SEM with 10–15 kV accelerating voltage and 8 mm working distance, the Spherical-aberration Corrected Field Emission Transmission Electron Microscope (HRTEM) image for PtSn nanoparticles was recorded. As for the TEM images, the samples were prepared by the drop of PtSn nanomaterials in toluene onto 200 mesh carbon-coated copper grids. Furthermore, the EDS was used to confirm the element for the nanowire. Also, XRD was prepared by drying the PtSn nanomaterials solution on Si substrates, and the pattern was obtained with the Shimadzu XRD-6000 diffractometer equipped with Cu Kα radiation. Surface morphology and thickness of the nanosheets were characterized using a commercial scanning probe microscope system (Bruker, model: Dimension ICON in National Tsing Hua University Instruments centre).

2.4. Electrochemical measurements

All of the electrochemical measurements were performed in a three-electrode system on a potentiostate (VMP3 from Biologic with Ec-lab software). All experiments were conducted with a saturated calomel electrode (SCE) (in alkaline media) or Ag/AgCl electrode (in acidic media) as the reference electrode, a glassy carbon (GC) electrode as the working electrode and a Pt wire as the counter electrode. The cyclic voltammetry (CV) measurements were performed at room temperature, and the electrolyte was purged with argon for 30 min prior to electrochemical measurements.

For the working electrodes fabrication, typically 3 mg of PtSn or commercial Pt catalysts was dispersed in 1.5 mL toluene and 15 μL Nafion solution (5 wt%) sonicated for 1 h to form a homogeneous catalyst ink with a concentration of 2 mg/mL. Then, 10 μL of the dispersion was loaded onto GC electrode. The concentrations of Pt in the catalyst inks were obtained by inductively coupled plasma mass spectrometer (ICP-MS).

For methanol oxidation reaction (MOR) or ethanol oxidation reaction (EOR) measurement in alkaline media, the aqueous solutions of 0.2 M KOH containing 0.2 M methanol or ethanol were used for the electrolytes. The working electrode was initially cycled between −1.0 V and 0.4 V at 50 mV s^{-1} in 0.2 M KOH for about 20 cycles removing the residues on catalyst surface. The MOR or EOR measurement was obtained by CV scans between −1.0 V and 0.4 V at 50 mV s^{-1}. Afterwards, the corresponding potential was held at −0.25 V during the chronoamperometry measurements in 0.2 M KOH and 0.2 M methanol or ethanol. On the other hand, for MOR or EOR measurement in acidic media, the aqueous solutions of 0.5 M H_2SO_4 containing 0.5 M methanol or ethanol were conducted as electrolytes. Similarly, prior to the electrochemical measurements, the catalyst coated electrodes were pre-treated between −0.2 V and 1.0 V at 50 mV s^{-1} in 0.5 M H_2SO_4 for about 20 cycles for removing the surface possible contaminants on catalyst, then

the MOR or EOR measurement was obtained by CV scans between −0.2 V and 1.0 V at 50 mV s^{-1}.

3. Results and discussion

3.1. Synthesis and characterization

PtSn nanosheets were fabricated via heating up the solution containing precursors and surfactants from 130 °C to 320 °C under Schlenk line system with an argon steam. After obtained without unconverted precursors by centrifugation, PtSn nanosheets were analysed by X-ray diffraction (XRD), which the result is shown in Fig. 1(a). With the comparison between nanosheets and standard database (JCPDS no. 89-2056), [54] all the analogue fingerprint diffraction peaks indicated the nanosheets as PtSn with a primitive hexagonal structure and the space group $P6_3$ with the following lattice parameters: a = 4.1 Å, b = 4.1 Å, c = 5.44 Å. The four main characteristic peaks for PtSn are at 25.05°, 30.021°, 41.793°, and 44.126°, which corresponded to crystal facets of (1 0 1), (0 1 1), (0 1 2), and (1 1 0). Also, Fig. 1(b) shows the simulation of layered PtSn. Furthermore, PtSn nanosheets were examined by X-ray photoelectron spectroscopy (XPS) analysis to explore the surface states. Shown in Fig. 1(c – e), the XPS spectrum indicated the nanosheets contained only Pt and Sn. The region of Pt 4f and that of Sn 3d are labelled, and all the binding energies have been corrected with C 1s as reference. Displayed in Fig. 1(d), the Sn 3d

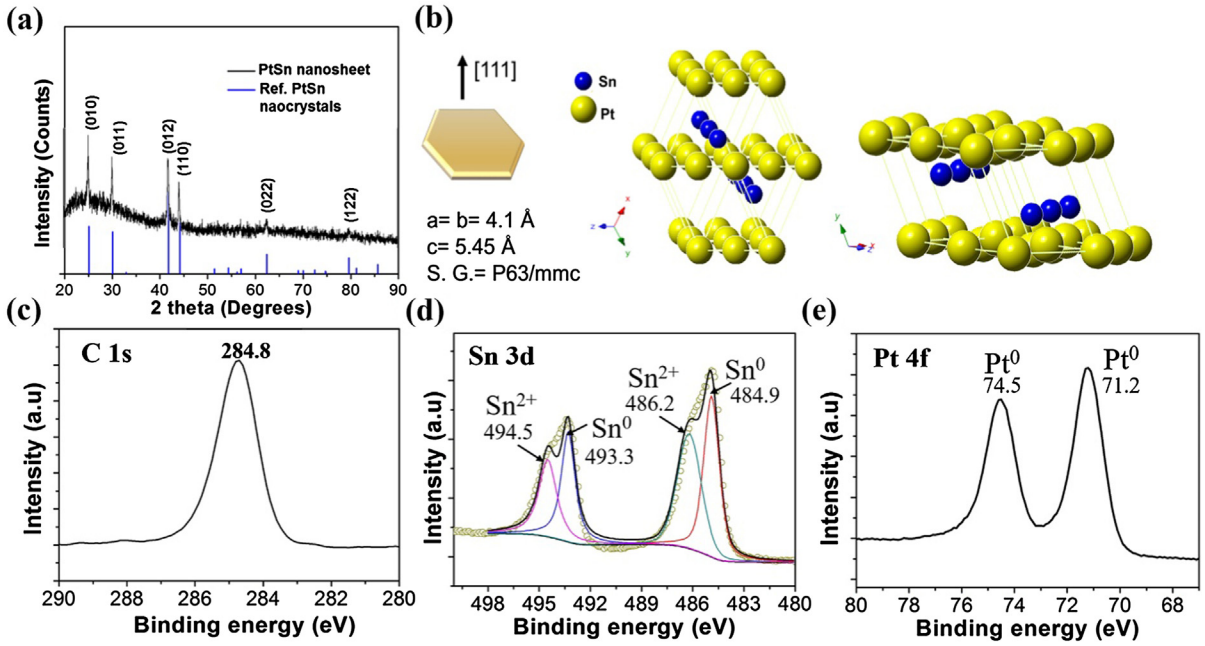

Fig. 1. (a) XRD pattern of PtSn nanosheets, (b) the simulated and piled nanosheets structures, (c-e) The XPS spectra of PtSn nanosheets: (c) C 1s, (d) Sn 3d, and (e) Pt 4f.

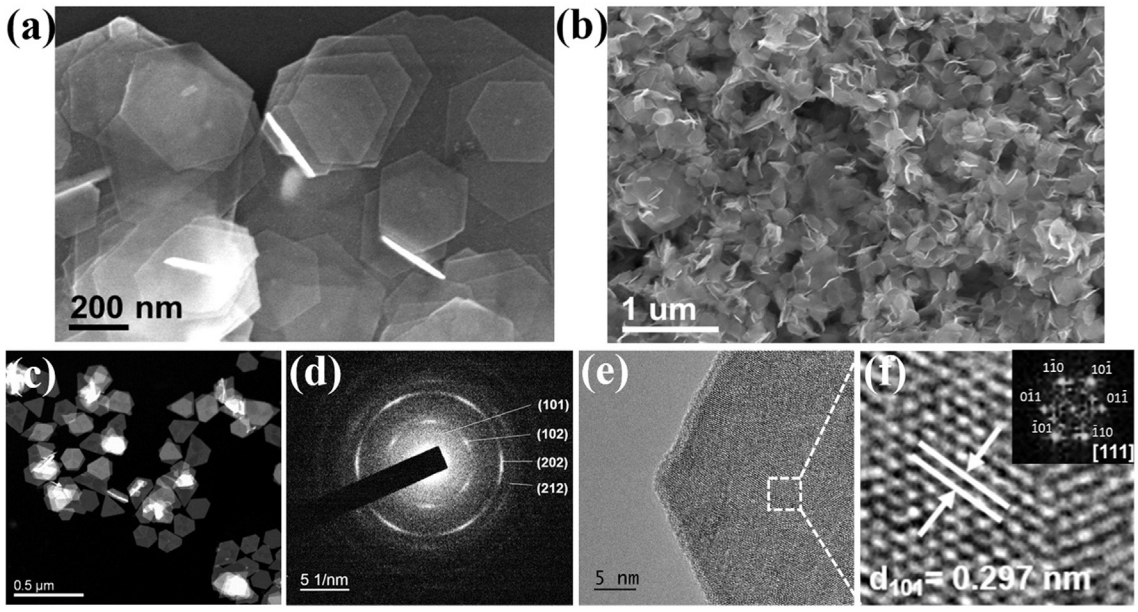

Fig. 2. (a and b) SEM images, (c) TEM image and (d) SAED image of PtSn nanosheets. (e, f) The HRTEM images of PtSn nanosheet, and FFT image is inserted.

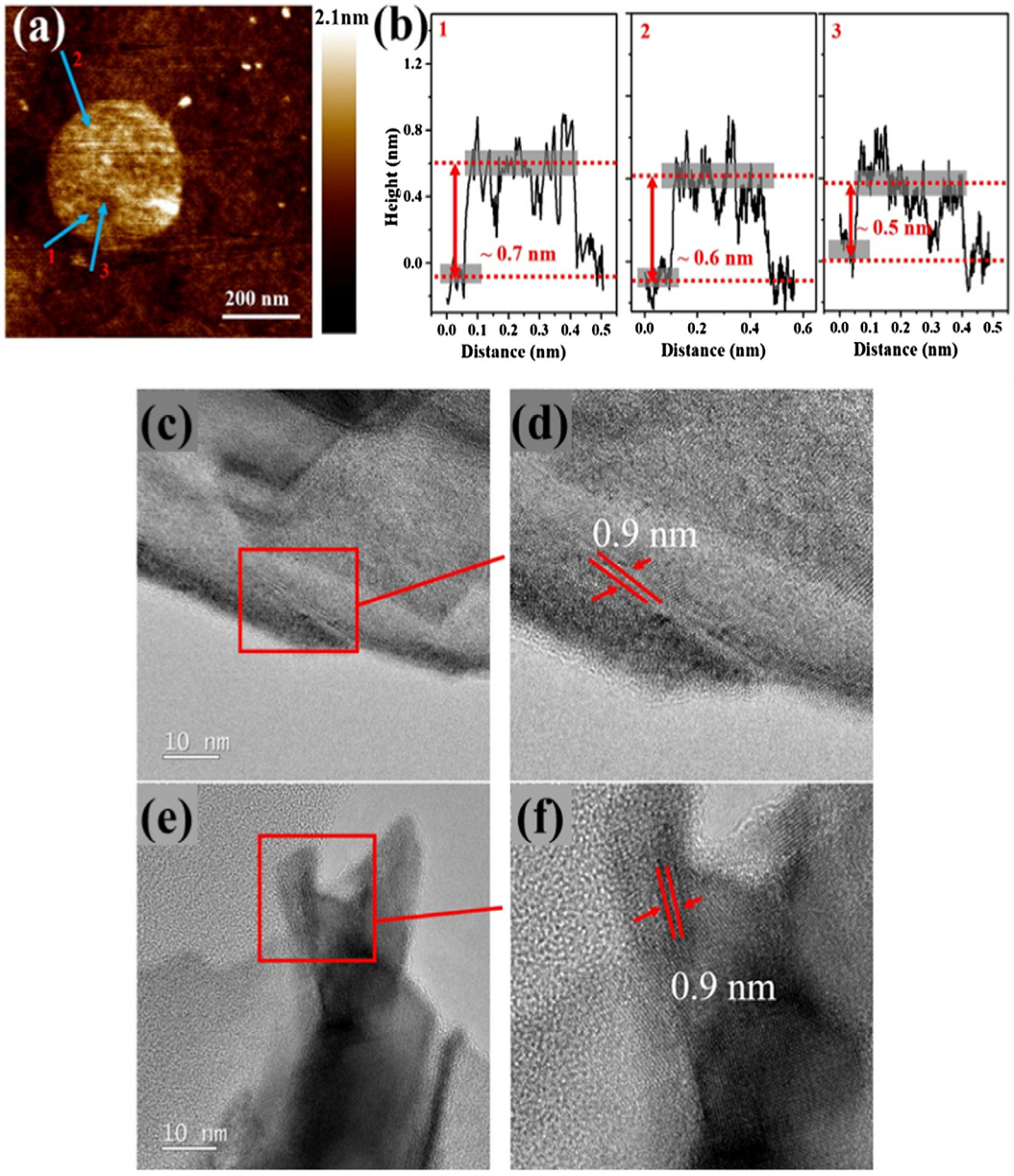

Fig. 3. (a, b) AFM image of a PtSn nanosheet (b) represents the results of thickness from AFM test in different directions, corresponding to the direction in (a). (c, f) The HRTEM images of PtSn nanosheet, and the measured thickness is displayed.

peaks contain two valence states, the +2 and 0. Both the valence states split into two peaks, peaks at 484.9 and 493.3 eV represent the +0 valence state, and peaks at 486.2 and 494.5 eV represent the +2 valence state. The appearance of the Sn +2 valence state indicated the surface of PtSn nanosheets are partially oxidised as SnO. Fig. 1(e) displayed the Pt 4f region, and the peak is split into two peaks at 71.2 and 74.5 eV.

The morphologies of synthesized PtSn nanosheets were observed by several electron microscopy analyses, including SEM, TEM and HRTEM. Fig. 2(a, b) are the SEM images with different magnifications, and the majority of these PtSn nanosheets are hexagonal structures. Furthermore, observed from SEM images, these nanosheets are easily piled one above another, and this might because of van der Waals force [55]. Also, these nanosheets have a wide diameter range from 200 nm to 1 μm. The dark field TEM image is displayed in Fig. 2(c), and the magnified SAED image is displayed in Fig. 2(d). From the SAED image, the four ring patterns of (0 1 1), (0 1 2), (0 2 2) and (1 2 2) facets appear on the surface of the nanosheets, which are corresponded to the peaks of 30.021°, 44.126°, 62.395°, and 79.562° in XRD database respectively. For further detailed morphologies of PtSn nanosheets, the HRTEM images were shown in Figs. 2(e, f) and S1. The diameter of the PtSn nanosheet shown in Fig. 2(e) is nearly 200 nm, and the measured two lattice d-spacings are 0.297 nm and 0.205 nm, corresponding to the crystal facets (0 1 1) and (1 1 0). Furthermore, the corresponding Fast Fourier Transform (FFT) (inserted in Fig. 2 (f)) also displayed the (0 1 1) and (1 1 0) crystal facets appear on the surface of PtSn nanosheets, which indicate the two main growing facets are the (0 1 1) and (1 1 0) crystal facets. The STEM and EDS mapping results double confirm that the nanosheets contained only Pt and Sn and which are with even element distribution (Fig. S2). From the SEM images above, the varied range of the PtSn nanosheet diameter and many studies suggest a possible synthetic mechanism [56–59]. The well dissolved tin solution was injected

into the platinum precursor solution; the forming intermediates would be thermal decompose at high temperature and the nucleate PtSn with hexagonal planar structure. The decomposed intermediates dissolved in the nucleus lead to the growth of the nanosheets; and under the surfactant environment, the nucleus have six facet growth direction that maintain the hexagonal structure. During the overall synthesis, the nucleation and the growth continuing competing, which in the SEM images, the wide diameter ranges of the nanosheets support the hexagonal nucleation and growth mechanism. However, this synthesis mechanism hypothesis would still need to be further analysed and confirmed.

The thickness of the nanosheets is crucial for 2D material since it would affect the surface energy density and volume to surface ratio. Here, the Fig. 3(a and b) shows the typical atomic force microscope (AFM) images for the PtSn nanosheets. From the AFM measurement, the thickness of nanosheets is around 0.6 nm. Also, as displayed in Fig. S3, the single nanosheet or one from the stacked nanosheets obtain a average thickness that under 1 nm as well. However, even though AFM is one of the most accurate thickness measure instruments, its limits still remained in measuring ultrathin thickness under few nanometers. Also, from the SEM images, these nanosheets tend to be piled instead of separated, which might because of Van der Waal force as discussed in previous paragraphed [60–62]. Moreover, when analysis with AFM, we found out that not only the sample solution concentration would affect the piling phenomenon, but also these nanosheets would

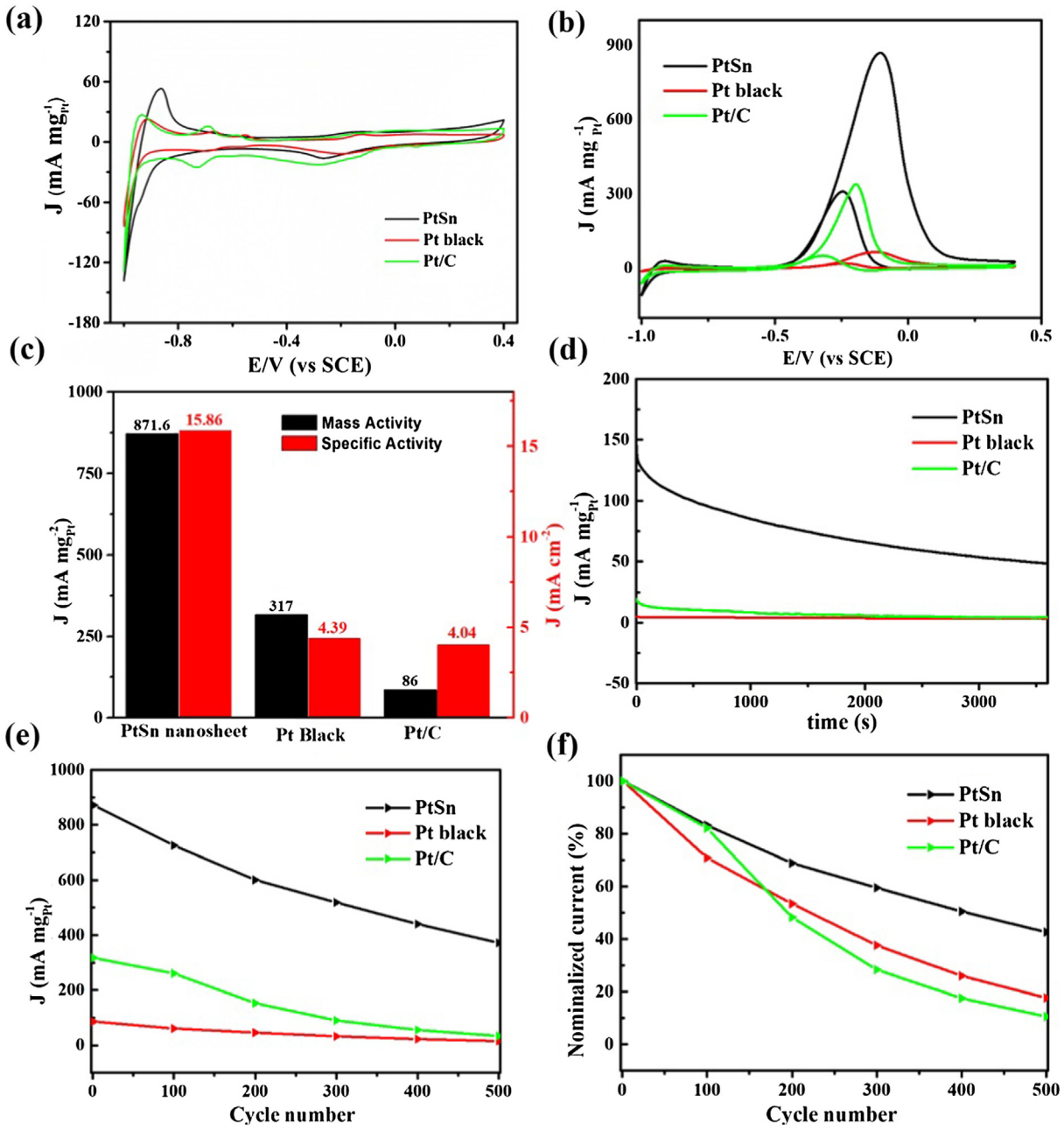

Fig. 4. Electrochemistry and MOR performance of the PtSn nanosheet, commercial Pt black and Pt/C. (a) CVs of these three catalysts in 0.2 M KOH aqueous solution at scan rate of 50 mV s^{-1}, (b) MOR curves of these three catalysts in 0.2 M KOH + 0.2 M CH_2OH at scan rate of 50 mV s^{-1}, (c) mass and specific activities of these three catalysts at their corresponding peak potentials in the CV curves in (b), and (d) J–t curves of PtSn nanosheet, commercial Pt black and Pt/C at 0.25 V (vs SCE). (e, f) Durability comparison of these three catalysts."J" represents the mass current density.

pack more severe when approaching to the wafer edges. In order to confirm the thickness of PtSn nanosheets which under 1 nm certainly, the PtSn nanosheets were also analysed under HRTEM (shown in Fig. 3(c–f)). From the HRTEM cross view, it is very clear that the most of the nanosheets are stacking on one another, and which these nanosheets obtain around 0.9 nm thickness. Hence, according to the measured evidence provided by both AFM and HRTEM, the average thickness of PtSn nanosheets is confirmed as under 1 nm.

3.2. Methanol oxidation reaction (MOR)

PtSn has caught attention in the usage as electrocatalyst for MOR and EOR. The electrocatalyst activity of MOR was examined in the standard electrochemical arrangement with the working electrode prepared by drop coating the PtSn nanoink onto a 0.196 cm^2 rotating disk electrode in an aqueous solution of KOH (0.2 M) and CH_2OH (0.2 M) at room temperature with the scan rate of 50 mV s^{-1} (results are shown in Fig. 4). The result of the cyclic voltammetry (CV) examination is displayed and normalized by the amount of Pt as the catalyst loading on the electrode. The electrochemical surface area (ECSA) was measured from the area of the hydrogen adsorption–desorption peaks after correcting for the double layer charging current from the CV (Fig. 4(a)) [63]. The ECSA value of the PtSn is calculated to be 66 m^2 g^{-1} of Pt, which is higher than that of Pt black (24.8 m^2 g^{-1}) and Pt/C (28.6 m^2 g^{-1}). Note that the higher ECSA value of a catalyst indicating that it poses higher electrocatalytic activity. Therefore, it is expected that Ptsn have a higher electrocatalytic activity than pure Pt on the glass carbon (GC) electrode.

Furthermore, the mass activity of PtSn nanosheets in MOR is the highest (871.6 mA mg_{Pt}^{-1}) by comparing to Pt/C (371 mA mg_{Pt}^{-1}) and Pt black (86.1 mA mg_{Pt}^{-1}) with the reactive work potential in the range of −1.0 to 0.45 V (vs SCE) (shown in Fig. 4(b)), which is 10.1 times and 2.3 times higher than Pt black and Pt/C catalysts respectively (shown in Fig. 4(c)). Also, shown in Figs. S4(d) and 4 (c), the specific activity of PtSn (15.86 mA cm^{-2}) as electrocatalyst in MOR is 3.6 times and 3.9 times higher than commercial Pt black (4.39 mA cm^{-2}) and Pt/C (4.04 mA cm^{-2}) catalysts. Furthermore, the electrocatalytic stability of PtSn nanosheets was also investigated by the amperometric measurement at the work potential of −0.25 V (vs SCE) (shown in Fig. 4(d)) and a continues 500-cycles CV sweeps test (exhibited in Figs. 4(e, f) and S4(a–c, e–f)). The mass activity of PtSn still remained as the highest compared to commercial Pt Black and Pt/C catalysts after 3600-seconds-amperometric measurement. On the other hand, after 500-cycles CV sweeps, mass activity of PtSn remained 48% of its initial value, while the retention of commercial Pt/C and Pt black are only 17.6% and 10.6% of their initial value (shown in Fig. 4(f)). These results of the retention value have demonstrated the enhanced the MOR-catalyst-activity durability of the PtSn nanosheets. The enhanced performance might be owing to the larger volume-surface ratio that leads to more reaction area are exposed.

The area distribution of PtSn nanosheets on electrodes would also affect the electrocatalystic performance. Exhibited in Figs. S5 and S6(b – e), different concentrations of PtSn nanoink, 4 mg/mL, 2 mg/mL and 0.5 mg/mL, were examined and the SEM images (Fig. S5(a – c)) were also displayed. From Fig. S5(d), the concentration of 2 mg/mL nanoink shows the highest activity among all the concentrations. Compared with the SEM images (Fig. S5(a – c)), the PtSn nanosheets would aggregate more vigorous in concentration of 0.5 mg/mL than 2 mg/mL, and the nanosheets is more likely to pile on one another in the higher concentration 4 mg/mL. Previous researchers have illustrated the importance of solution concentration in products' dispersion [64,65]. The nanosheets would aggregate while the concentration is too dilute or too high, only the appropriate concentration would perform better dispersion of the nanosheets. Furthermore, the degree of dispersion of the nanosheets would affect the active surface area revealing in the electrocatalystic test, and would affect the catalystic performance. As a result, the appropriate concentration of 2 mg/mL would demonstrate better performance in electrochemical examinations.

Furthermore, MOR in acid media (aqueous solution of 0.5 M H_2SO_4 and 0.5 M CH_2OH) also have been studied at 50 mV s^{-1},

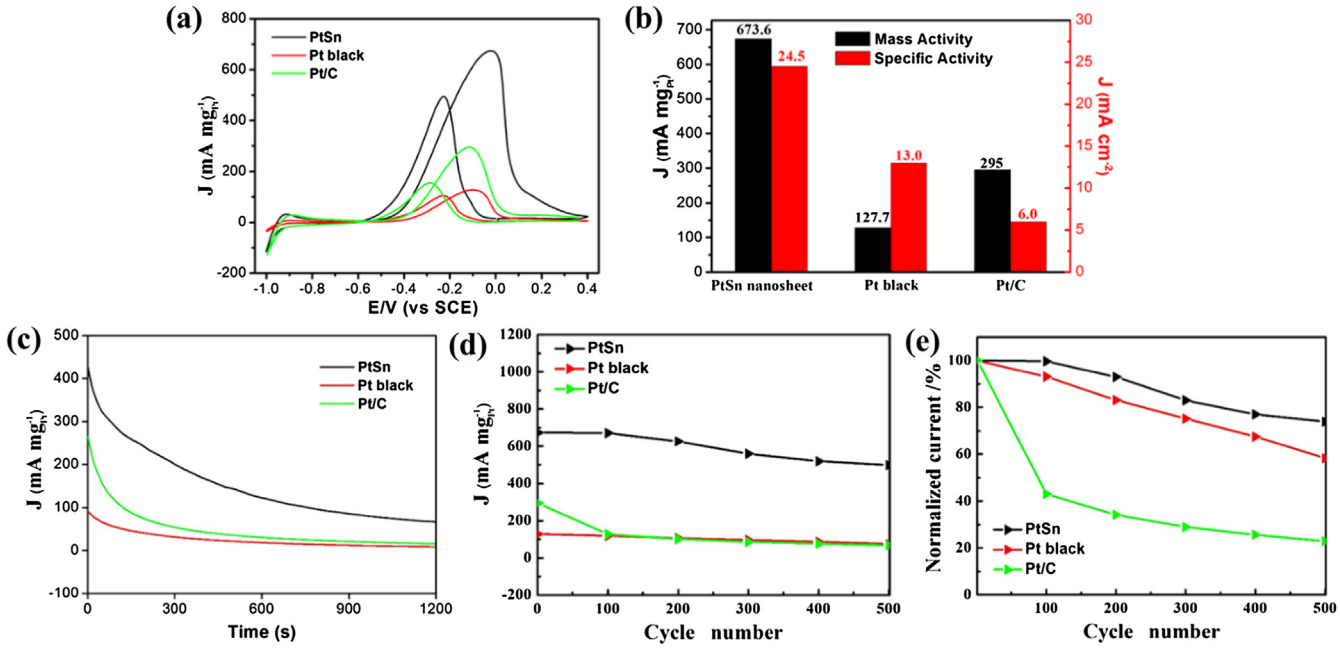

Fig. 5. Electrochemistry and EOR performance of the PtSn nanosheet, commercial Pt black and Pt/C. (a) EOR curves of these three catalysts in 0.2 M KOH + 0.2 M C_2H_5OH at scan rate of 50 mV s^{-1}, (b) mass and specific activities of these three catalysts at their corresponding peak potentials in the CV curves in (a), and (c) J–t curves of PtSn nanosheet, commercial Pt black and Pt/C at 0.25 V (vs SCE). (d,e) Durability comparison of these three catalysts.

Table 1
Comparison of various PtSn related catalysts.

Catalyst	Reaction	Electrolyte	Cathodic peak current density (mA/cm^2) vs pure Pt	Cathodic peak current density (mA/cm^2) vs Pt/C	Cathodic peak mass activity (mA/mg_{Pt}) vs pure Pt	Cathodic peak mass activity (mA/mg_{Pt}) vs Pt/C	Ref.
PtSn nanosheets	MOR	0.5 M H_2SO_4 + 0.5 M methanol	3.6 times	3.9 times	10.1 times	2.3 times	This work
	EOR	0.2 M KOH + 0.2 M ethanol	2.2 times	4.1 times	5.3 times	2.3 times	
PtSn/XC-72	EOR	0.5 M H_2SO_4 + 1.0 M ethanol	–	–	–	2.0 times	[66]
PtSn/rGO			–	–	–	1.8 times	
PtSn/CNT			–	–	–	1.7 times	
PtSn nanoparticles	MOR	1.0 M H_2SO_4 + 0.5 M methanol	1.7 times	–	–	–	[11]
Cubic PtSn	MOR	0.5 M H_2SO_4 + 0.5 M methanol	0.9 times	–	–	–	[9]
Hierarchical PtSn			1.9 times	–	–	–	
Excavated cubic PtSn			2.1 times	–	–	–	
PtSn thin films	MOR	0.5 M H_2SO_4 + 0.5 M methanol	1.5 times	–	–	–	[70]
PtSn/C	MOR	0.5 M H_2SO_4 + 1.0 M methanol	–	1.3 times	–	–	[46]
	EOR	0.5 M H_2SO_4 + 1.0 M ethanol	–	2.9 times	–	–	
PtSn/CNT(A)&(B)	EOR	1.0 M $HClO_4$ + 1.0 M ethanol	–	1.9 & 1.7 times	–	–	[68]
$PtSnO_2$/CNT			–	1.3 times	–	–	
PtSn/PEI-MWCNTs	EOR	0.5 M H_2SO_4 + 1.0 M ethanol	–	1.9 times	–	–	[69]

and the representative CVs are shown in Fig. S6(a). The mass peak current density (normalized to the mass of Pt) of PtSn nanosheets (10.89 mA cm^{-2}) is almost 2.5 times higher than that of Pt/C (4.3 mA cm^{-2}). These fascinating findings indicate that PtSn nanosheets can perform EOR at both alkaline and have a much higher mass catalytic activity than Pt black and commercial Pt/C generated.

3.3. Ethanol oxidation reaction (EOR)

EOR was measured by CV in an aqueous solution of 0.2 M KOH and 0.2 M C_2H_5OH at room temperature and scan rate of 50 mV s^{-1}. The current density of each CV curve is normalized against the Pt loading on the electrode, and a significant difference in catalytic activity of the different catalysts can be clearly observed. The CV curve of PtSn nanosheets shows much stronger hydrogen absorption peak compared to the commercial Pt black and Pt/C catalysts (Fig. 5(a)), indicating the larger electrochemical active surface area in comparison with the commercial Pt black and Pt/C catalysts. Also, the PtSn nanosheets exhibit highest current for EOR at reactive work potential in the range of 0.4 to −0.1 V (vs SCE) (Fig. 5(b)), with the corresponding peak potential of 673.6 mA mg_{Pt}^{-1}, which is 5.3 times that of commercial Pt black (127.7 mA mg_{Pt}^{-1}) and 2.3 times that of commercial Pt/C catalyst (295 mA mg_{Pt}^{-1}) (Fig. 5(c)). The electrocatalytic stability of PtSn nanosheets was also investigated by the amperometric measurement at the work potential of −0.25 V (vs SCE) (Fig. 5d) and after the electrocatalytic EOR proceeded for 1200 s, PtSn nanosheets kept 16% of its initial response current while the commercial Pt black and Pt/C catalysts showed almost no response current, suggesting the higher electrocatalytic stability of PtSn nanosheets compared to the commercial Pt black and Pt/C at alkaline condition. We also carried out the EOR durability tests of these three catalysts. (Fig. 5(e and f) and Fig. S7). The mass activity of PtSn nanosheets maintained for 73.9% of its initial value, while the commercial Pt black and Pt/C maintained only 58.2% and 22.8% mass activities after 500 sweeping cycles respectively, highlighting the enhanced catalytic durability of the PtSn nanosheets. Furthermore, EOR in acid media (aqueous solution of 0.5 M H_2SO_4 and C_2H_5OH) also have been studied at 50 mV s^{-1}, and the representative CVs are shown in Fig. S8(a). The mass peak current density (normalized to the mass of Pt) of PtSn nanosheets (292.6 mA $mg_{Pt}{}^{-1}$) is almost 4.9 times higher than that of Pt black (60 mA mg_{Pt}^{-1}) and 2.0 times higher than that of commercial Pt/C (143.4 mA mg_{Pt}^{-1}) (Fig. S8(b)). These fascinating findings indicate that PtSn nanosheets can perform EOR at both alkaline and have a much higher mass catalytic activity than Pt black and commercial Pt/C generated.

Previous studies of PtSn related electrocatalysts for MOR and EOR are listed and compared in Table 1, such as PtSn nanoparticles, PtSn thin film, and PtSn with support [9–11,66–70]. PtSn nanosheets exhibit higher amplification of catalytic activity than PtSn in other different morphologies. When compared with the PtSn system, the nanosheets have the highest activity as electrocatalyst. The extraordinary performance of PtSn nanosheets as electorcatalyst in both EOR and MOR may be due to its 2D structure. In the past decade, many studies have indicated that the crucial advantage of 2D material is that all the catalytically active sites are expose [71]. In nanosheets, since the thickness is below one nanometre, all the surface and active sites can be seen as all exposed. Furthermore, the simulation of PtSn nanosheets, displayed in Fig. 1(b), indicates the (1 1 1) crystal facet is the dominate site expose in the surface. Previous studies have verified that the adsorption of CO and OH is strongly prefer on (1 1 1) facets of Pt [72]. With the strong and large active site of (1 1 1) facets

exposed, nanosheet displayed the highest amplification of catalytic activity among all the different PtSn morphologies.

4. Conclusion

In summary, we have developed a facile colloid synthesis method for the preparation of ultrathin PtSn nanosheets with thickness ranging from 0.6 to 0.9 nm. As electrocatalysts in MOR and EOR examination, PtSn nanosheets not only exhibit an outstanding mass activity in MOR (871.6 mA mg_{Pt}^{-1}), which is 2.3 times (371 mA mg_{Pt}^{-1}) and 10.1 times (86.1 mA mg_{Pt}^{-1}) higher than that of commercial Pt/carbon and Pt black respectively, but also display a mass activity in EOR (673.6 mA mg_{Pt}^{-1}) with 5.3 times higher commercial Pt black (127.7 mA mg_{Pt}^{-1}) and 2.3 times higher than commercial Pt/C catalyst (295 mA mg_{Pt}^{-1}). By comparing to the previous studies of PtSn with different morphologies or carbon supports, the improved performance may be due to the large area of (1 1 1) facet sites. PtSn nanosheets exhibited good electro-oxidation properties for MOR and EOR in both acidic and alkaline environment, owing to their ultrathin 2D structure dramatically enhance the cleavage of C—C bond but also improve the removal of CO_{ads} species formed on the platinum surface during alcohol electro-oxidation. Their high current densities, enhanced durability and relatively higher efficiency compared to commercial Pt catalysts will provide a motivation to extend synthesis of other ultrathin 2D nanomaterials with desired functions in the development of high-performance catalyst systems.

Acknowledgements

We acknowledge the financial support by the Ministry of Science and Technology through the grants of MOST 106- 2221-E-007-081-MY3, 106-2628-E-007-005-MY3, and 103- 2221-E-007-089-MY3, and MOST 106-2622-8-007-017, and by National Tsing Hua University through the grant of 107Q2708E1.

Appendix A. Supplementary material

Supplementary data to this article can be found online at https://doi.org/10.1016/j.jcis.2019.02.082.

References

[1] L.Z. Bu, S.J. Guo, X. Zhang, X. Shen, D. Su, G. Lu, X. Zhu, J.L. Yao, J. Guo, X.Q. Huang, Surface engineering of hierarchical platinum-cobalt nanowires for efficient electrocatalysis, Nat. Commun. 7 (2016) 11850.
[2] T. Gunji, T. Tanabe, A.J. Jeevagan, S. Usui, T. Tsuda, S. Kaneko, G. Saravanan, H. Abe, F. Matsumoto, Facile route for the preparation of ordered intermetallic Pt_3Pb-PtPb core-shell nanoparticles and its enhanced activity for alkaline methanol and ethanol oxidation, J. Power Sources 273 (2015) 990–998.
[3] W.X. Du, G.X. Yang, E. Wong, N.A. Deskins, A.I. Frenkel, D. Su, X.W. Teng, Platinum-tin oxide core-shell catalysts for efficient electro-oxidation of ethanol, J. Am. Chem. Soc. 136 (31) (2014) 10862–10865.
[4] Z.P. Xiong, S.M. Li, H. Xu, K. Zhang, B. Yan, Y.K. Du, Newly designed ternary metallic PtPdBi hollow catalyst with high performance for methanol and ethanol oxidation, Catalysts 7 (7) (2017) 208.
[5] B. Jiang, C. Li, J. Tang, T. Takei, J.H. Kim, Y. Ide, J. Henzie, S. Tominaka, Y. Yamauchi, Tunable-sized polymeric micelles and their assembly for the preparation of large mesoporous platinum nanoparticles, Angew. Chem. Int. Ed. 55 (34) (2016) 10037–10041.
[6] B. Jiang, C. Li, V. Malgras, M. Imura, S. Tominaka, Y. Yamauchi, Mesoporous Pt nanospheres with designed pore surface as highly active electrocatalyst, Chem. Sci. 7 (2) (2016) 1575–1581.
[7] H.S. Wang, Z. Jusys, R.J. Behm, H.D. Abruna, New insights into the mechanism and kinetics of adsorbed CO electrooxidation on platinum: online mass spectrometry and kinetic monte carlo simulation studies, J. Phys. Chem. C 116 (20) (2012) 11040–11053.
[8] M.H. Shao, R.R. Adzic, Electrooxidation of ethanol on a Pt electrode in acid solutions: in situ ATR-SEIRAS study, Electrochim. Acta 50 (12) (2005) 2415–2422.
[9] Q. Chen, Y. Yang, Z. Cao, Q. Kuang, G. Du, Y. Jiang, Z. Xie, L. Zheng, Excavated cubic platinum–tin alloy nanocrystals constructed from ultrathin nanosheets with enhanced electrocatalytic activity, Angew. Chem. Int. Ed. 55 (31) (2016) 9021–9025.
[10] D.-H. Kwak, Y.-W. Lee, S.-B. Han, E.-T. Hwang, H.-C. Park, M.-C. Kim, K.-W. Park, Ultrasmall PtSn alloy catalyst for ethanol electro-oxidation reaction, J. Power Sources 275 (2015) 557–562.
[11] L. Zheng, L. Xiong, J. Sun, J. Li, S. Yang, J. Xia, Capping agent free synthesis of PtSn bimetallic nanoparticles with enhanced electrocatalytic activity and lifetime over methanol oxidation, Catal. Commun. 9 (5) (2008) 624–629.
[12] H.C. Peng, W.H. Qi, H.F. Wu, J.T. He, Y.J. Li, H.P. Xie, One-pot synthesis of CuPt nanodendrites with enhanced activity towards methanol oxidation reaction, RSC Adv. 8 (17) (2018) 9293–9298.
[13] T.Y. Liu, K. Wang, Q. Yuan, Z.B. Shen, Y. Wang, Q.H. Zhang, X. Wang, Monodispersed sub-5.0 nm PtCu nanoalloys as enhanced bifunctional electrocatalysts for oxygen reduction reaction and ethanol oxidation reaction, Nanoscale 9 (9) (2017) 2963–2968.
[14] Y.G. Zhao, J.J. Liu, C.G. Liu, F. Wang, Y. Song, Amorphous CuPt alloy nanotubes induced by $Na_2S_2O_3$ as efficient catalysts for the methanol oxidation reaction, ACS Catal. 6 (7) (2016) 4127–4134.
[15] R.M. Altarawneh, P.G. Pickup, Pt and PtRu catalyst bilayers increase efficiencies for ethanol oxidation in proton exchange membrane electrolysis and fuel cells, J. Power Sources 366 (2017) 27–32.
[16] D. Bin, F.F. Ren, H.W. Wang, K. Zhang, B.B. Yang, C.Y. Zhai, M.S. Zhu, P. Yang, Y. K. Du, Facile synthesis of PVP-assisted PtRu/RGO nanocomposites with high electrocatalytic performance for methanol oxidation, RSC Adv. 4 (74) (2014) 39612–39618.
[17] M. Chatterjee, A. Chatterjee, S. Ghosh, I. Basumallick, Electro-oxidation of ethanol and ethylene glycol on carbon-supported nano-Pt and -PtRu catalyst in acid solution, Electrochim. Acta 54 (28) (2009) 7299–7304.
[18] Z.L. Liu, F.B. Su, X.H. Zhang, S.W. Tay, Preparation and characterization of PtRu nanoparticles supported on nitrogen-doped porous carbon for electrooxidation of methanol, ACS Appl. Mater. Inter. 3 (10) (2011) 3824–3830.
[19] S.L. Lu, K. Eid, D.H. Ge, J. Guo, L. Wang, H.J. Wang, H.W. Gu, One-pot synthesis of PtRu nanodendrites as efficient catalysts for methanol oxidation reaction, Nanoscale 9 (3) (2017) 1033–1039.
[20] Y.N. Wu, S.J. Liao, H.F. Guo, X.Y. Hao, High-performance Pd@PtRu/C catalyst for the anodic oxidation of methanol prepared by decorating Pd/C with a PtRu shell, J. Power Sources 224 (2013) 66–71.
[21] L. Li, C.X. Tian, J.S. Yang, X.H. Zhang, J.H. Chen, One-pot synthesis of PtRh/beta-CD-CNTs for methanol oxidation, Int. J. Hydr. Energy 40 (43) (2015) 14866–14874.
[22] Q.Q. Lu, J.S. Huang, C. Han, L.T. Sun, X.R. Yang, Facile synthesis of composition-tunable PtRh nanosponges for methanol oxidation reaction, Electrochim. Acta 266 (2018) 305–311.
[23] Y. Shen, B. Gong, K.J. Xiao, L. Wang, In situ assembly of ultrathin PtRh nanowires to graphene nanosheets as highly efficient electrocatalysts for the oxidation of ethanol, ACS Appl. Mater. Inter. 9 (4) (2017) 3535–3543.
[24] Y.W. Lee, S.W. Han, K.Y. Lee, Site-selectively Pt-decorated PdPt bimetallic nanosheets characterized by electrocatalytic property for methanol oxidation, Mater. Chem. Phys. 214 (2018) 201–208.
[25] Y. Liu, M.F. Chi, V. Mazumder, K.L. More, S. Soled, J.D. Henao, S.H. Sun, Composition-controlled synthesis of bimetallic PdPt nanoparticles and their electro-oxidation of methanol, Chem. Mater. 23 (18) (2011) 4199–4203.
[26] Y.X. Pan, X.Y. Guo, M.Z. Li, Y.H. Liang, Y.P. Wu, Y. Wen, H.F. Yang, Construction of dandelion-like clusters by PtPd nanoseeds for elevating ethanol eletrocatalytic oxidation, Electrochim. Acta 159 (2015) 40–45.
[27] P.T. Qiu, S.M. Lian, G. Yang, S.C. Yang, Halide ion-induced formation of single crystalline mesoporous PtPd bimetallic nanoparticles with hollow interiors for electrochemical methanol and ethanol oxidation reaction, Nano Res. 10 (3) (2017) 1064–1077.
[28] M. D'Villa-Silva, F.C. Simoes, R.F.B. de Souza, J.C.M. Silva, M.C. Santos, Comparative studies of oxygen reduction reaction and ethanol oxidation reaction on PtSn/C and PtNi/C catalysts, ECS Trans. 41 (1) (2011) 1299–1306.
[29] Q.A. Jiang, L.H. Jiang, H.Y. Hou, J. Qi, S.L. Wang, G.Q. Sun, Promoting effect of Ni in PtNi bimetallic electrocatalysts for the methanol oxidation reaction in alkaline media: experimental and density functional theory studies, J. Phys. Chem. C 114 (46) (2010) 19714–19722.
[30] C.Z. Wang, Y. Zhang, Y.J. Zhang, P. Xu, C.M. Feng, T. Chen, T. Guo, F.N. Yang, Q. Wang, J.X. Wang, M.T. Shi, L.Z. Fan, S.W. Chen, Highly ordered hierarchical Pt and PtNi nanowire arrays for. enhanced electrocatalytic activity toward methanol oxidation, ACS Appl. Mater. Inter. 10 (11) (2018) 9444–9450.
[31] R.P. Xiu, F.F. Zhang, Z.H. Wang, M. Yang, J.F. Xia, R.J. Gui, Y.Z. Xia, Electrodeposition of PtNi bimetallic nanoparticles on three-dimensional graphene for highly efficient methanol oxidation, RSC Adv. 5 (105) (2015) 86578–86583.
[32] P. Yang, X. Yuan, H. Hu, Y. Liu, H. Zheng, D. Yang, L. Chen, M. Cao, Y. Xu, Y. Min, Solvothermal synthesis of alloyed PtNi colloidal nanocrystal clusters (cncs) with enhanced catalytic activity for methanol oxidation, Adv. Funct. Mater. 28 (1) (2018) 1704774.
[33] K. Artyushkova, B. Halevi, M. Padilla, P. Atanassov, E.A. Baranova, Mechanistic study of electrooxidation of ethanol on ptsn nanoparticles in alkaline and acid media, J. Electrochem. Soc. 162 (6) (2015) H345–H351.
[34] J. Maya-Cornejo, R. Carrera-Cerritos, D. Sebastian, J. Ledesma-Garcia, L.G. Arriaga, A.S. Arico, V. Baglio, PtCu catalyst for the electro-oxidation of ethanol in an alkaline direct alcohol fuel cell, Int. J. Hydr. Energy 42 (46) (2017) 27919–27928.

[35] S.B. Adler, Factors governing oxygen reduction in solid oxide fuel cell cathodes, Chem. Rev. 104 (10) (2004) 4791–4843.
[36] L. Liu, G. Samjeske, S. Nagamatsu, O. Sekizawa, K. Nagasawa, S. Takao, Y. Imaizumi, T. Yamamoto, T. Uruga, Y. Iwasawa, Enhanced oxygen reduction reaction activity and characterization of Pt-Pd/C bimetallic fuel cell catalysts with Pt-enriched surfaces in acid media, J. Phys. Chem. C 116 (44) (2012) 23453–23464.
[37] Z.Y. Zhang, L. Xin, K. Sun, W.Z. Li, Pd-Ni electrocatalysts for efficient ethanol oxidation reaction in alkaline electrolyte, Int. J. Hydr. Energy 36 (20) (2011) 12686–12697.
[38] Y.S. Kim, S.H. Nam, H.S. Shim, H.J. Ahn, M. Anand, W.B. Kim, Electrospun bimetallic nanowires of PtRh and PtRu with compositional variation for methanol electrooxidation, Electrochem. Commun. 10 (7) (2008) 1016–1019.
[39] X. Zhao, M. Yin, L. Ma, L. Liang, C. Liu, J. Liao, T. Lu, W. Xing, Recent advances in catalysts for direct methanol fuel cells, Energy Environ. Sci. 4 (8) (2011) 2736–2753.
[40] Q. Lu, L. Sun, X. Zhao, J. Huang, C. Han, X. Yang, One-pot synthesis of interconnected $Pt_{95}Co_5$ nanowires with enhanced electrocatalytic performance for methanol oxidation reaction, Nano Res. 11 (5) (2018) 2562–2572.
[41] H. Liu, C. Li, D. Chen, P. Cui, F. Ye, J. Yang, Uniformly dispersed platinum-cobalt alloy nanoparticles with stable compositions on carbon substrates for methanol oxidation reaction, Sci. Rep. 7 (1) (2017) 11421.
[42] S.C. Zignani, V. Baglio, E.R. Gonzalez, A.S. Arico, Durability of a PtSn ethanol oxidation electrocatalyst, Chemelectrochem. 1 (8) (2014) 1403–1406.
[43] Y.J. Ma, H. Wang, S. Ji, V. Linkov, R.F. Wang, PtSn/C catalysts for ethanol oxidation: the effect of stabilizers on the morphology and particle distribution, J. Power Sources 247 (2014) 142–150.
[44] R.B. Kutz, B. Braunschweig, P. Mukherjee, R.L. Behrens, D.D. Dlott, A. Wieckowski, Reaction pathways of ethanol electrooxidation on polycrystalline platinum catalysts in acidic electrolytes, J. Catal. 278 (2) (2011) 181–188.
[45] W.J. Zhou, S.Q. Song, W.Z. Li, Z.H. Zhou, G.Q. Sun, Q. Xin, S. Douvartzides, P. Tsiakaras, Direct ethanol fuel cells based on PtSn anodes: the effect of Sn content on the fuel cell performance, J. Power Sources 140 (1) (2005) 50–58.
[46] D.H. Lim, D.H. Choi, W.D. Lee, H.I. Lee, A new synthesis of a highly dispersed and CO tolerant PtSn/C electrocatalyst for low-temperature fuel cell; its electrocatalytic activity and long-term durability, Appl. Catal. B-Environ. 89 (3–4) (2009) 484–493.
[47] E.E. Switzer, T.S. Olson, A.K. Datye, P. Atanassov, M.R. Hibbs, C.J. Cornelius, Templated Pt-Sn electrocatalysts for ethanol, methanol and CO oxidation in alkaline media, Electrochim. Acta 54 (3) (2009) 989–995.
[48] F. Saleem, Z.C. Zhang, B. Xu, X.B. Xu, P.L. He, X. Wang, Ultrathin Pt-Cu Nanosheets and Nanocones, J. Am. Chem. Soc. 135 (49) (2013) 18304–18307.
[49] L. Zhang, L.T. Roling, X. Wang, M. Vara, M.F. Chi, J.Y. Liu, S.I. Choi, J. Park, J.A. Herron, Z.X. Xie, M. Mavrikakis, Y.N. Xia, Platinum-based nanocages with subnanometer-thick walls and well-defined, controllable facets, Science 349 (6246) (2015) 412–416.
[50] Q.L. Chen, Z.M. Cao, G.F. Du, Q. Kuang, J. Huang, Z.X. Xie, L.S. Zheng, Excavated octahedral Pt-Co alloy nanocrystals built with ultrathin nanosheets as superior multifunctional electrocatalysts for energy conversion applications, Nano Energy 39 (2017) 582–589.
[51] C.L. Tan, H. Zhang, Wet-chemical synthesis and applications of non-layer structured two-dimensional nanomaterials, Nat. Commun. 6 (2015) 7873.
[52] X.T. Du, Y. Yang, J. Liu, B. Liu, J.B. Liu, C. Zhong, W.B. Hu, Surfactant-free and template-free electrochemical approach to prepare well-dispersed Pt nanosheets and their high electrocatalytic activities for ammonia oxidation, Electrochim. Acta 111 (2013) 562–566.
[53] L. Dai, Y. Zhao, Q. Qin, X.J. Zhao, C.F. Xu, N.F. Zheng, Carbon-monoxide-assisted synthesis of ultrathin PtCu alloy nanosheets and their enhanced catalysis, Chemnanomat 2 (8) (2016) 776–780.
[54] J.C. Bauer, X. Chen, Q. Liu, T.-H. Phan, R.E. Schaak, Converting nanocrystalline metals into alloys and intermetallic compounds for applications in catalysis, J. Mater. Chem. 18 (3) (2008) 275–282.
[55] K. Novoselov, A. Mishchenko, A. Carvalho, A.C. Neto, 2D materials and van der Waals heterostructures, Science 353 (6298) (2016) aac9439.
[56] Y.H. Leng, Y.T. Wang, X.G. Li, T. Liu, S. Takahashhi, Controlled synthesis of triangular and hexagonal Ni nanosheets and their size-dependent properties, Nanotechnology 17 (19) (2006) 4834–4839.
[57] W. Han, M.Y. Gao, Investigations on iron sulfide nanosheets prepared via a single-source precursor approach, Cryst. Growth Des. 8 (3) (2008) 1023–1030.
[58] Z.C. Wang, Y.Z. Chen, D.Q. Zeng, Q.F. Zhang, D.L. Peng, Solution synthesis of triangular and hexagonal nickel nanosheets with the aid of tungsten hexacarbonyl, Crystengcomm 18 (8) (2016) 1295–1301.
[59] S. Kar, A. Dev, S. Chaudhuri, Simple solvothermal route to synthesize ZnO nanosheets, nanonails, and well-aligned nanorod arrays, J. Phys. Chem. B 110 (36) (2006) 17848–17853.
[60] J. Zhang, H.Y. Zhu, X.X. Wu, H. Cui, D.M. Li, J.R. Jiang, C.X. Gao, Q.S. Wang, Q.L. Cui, Plasma-assisted synthesis and pressure-induced structural transition of single-crystalline SnSe nanosheets, Nanoscale 7 (24) (2015) 10807–10816.
[61] K.J. Yang, J. Wang, B.L. Chen, Facile fabrication of stable monolayer and few-layer graphene nanosheets as superior sorbents for persistent aromatic pollutant management in water, J. Mater. Chem. A 2 (43) (2014) 18219–18224.
[62] X.D. Liu, Y.D. Han, H.Y. Jing, J. Wei, L.Y. Xu, Effect of graphene nanosheets reinforcement on the performance of Sn-Ag-Cu lead-free solder, Mat. Sci. Eng. A-Struct. 562 (2013) 25–32.
[63] L. Han, P.L. Cui, H.Y. He, H. Liu, Z.J. Peng, J. Yang, A seed-mediated approach to the morphology-controlled synthesis of bimetallic copper-platinum alloy nanoparticles with enhanced electrocatalytic performance for the methanol oxidation reaction, J. Power Sources 286 (2015) 488–494.
[64] S.N. Luoma, Processes affecting metal concentrations in estuarine and coastal marine sediments, heavy metals in the marine environment, CRC Press, 2017, pp. 51–66.
[65] J.R. Conway, A.S. Adeleye, J. Gardea-Torresdey, A.A. Keller, Aggregation, dissolution, and transformation of copper nanoparticles in natural waters, Environ. Sci. Tech. 49 (5) (2015) 2749–2756.
[66] F. Wu, D. Zhang, M. Peng, Z. Yu, X. Wang, G. Guo, Y. Sun, Microfluidic synthesis enables dense and uniform loading of surfactant-free PtSn nanocrystals on carbon supports for enhanced ethanol oxidation, Angew. Chem. Int. Ed. 55 (16) (2016) 4952–4956.
[67] W. Zhou, Z. Zhou, S. Song, W. Li, G. Sun, P. Tsiakaras, Q. Xin, Pt based anode catalysts for direct ethanol fuel cells, Appl. Catal. B-Environ. 46 (2) (2003) 273–285.
[68] H. Song, M. Luo, X. Qiu, G. Cao, Insights into the endurance promotion of PtSn/CNT catalysts by thermal annealing for ethanol electro-oxidation, Electrochim. Acta 213 (2016) 578–586.
[69] X. Geng, Y. Cen, R.D. Sisson, J. Liang, An effective approach towards the immobilization of PtSn nanoparticles on noncovalent modified multi-walled carbon nanotubes for ethanol electrooxidation, Energies 9 (3) (2016) 165.
[70] S.S. Sarmoor, S.J. Hoseini, R.H. Fath, M. Roushani, M. Bahrami, Facile synthesis of PtSnZn nanosheet thin film at oil-water interface by use of organometallic complexes: an efficient catalyst for methanol oxidation and p-nitrophenol reduction reactions, Appl. Organomet. Chem. 32 (1) (2018) e3979.
[71] D. Voiry, J. Yang, M. Chhowalla, Recent strategies for improving the catalytic activity of 2D TMD nanosheets toward the hydrogen evolution reaction, Adv. Mater. 28 (29) (2016) 6197–6206.
[72] L. Dai, S. Mo, Q. Qin, X. Zhao, N. Zheng, Carbon monoxide-assisted synthesis of ultrathin PtCu3 alloy wavy nanowires and their enhanced electrocatalysis, Small 12 (12) (2016) 1572–1577.